ACS Catalysis

pubs.acs.org/acscatalysis

Research Article

Highly Efficient Supramolecular Photocatalysts for CO_2 Reduction with Eight Carbon−Carbon Bonds between a Ru(II) Photosensitizer and a Re(I) Catalyst Unit

Kei Kamogawa, Antonio Santoro, Ambra M. Cancelliere, Yuushi Shimoda, Kiyoshi Miyata, Ken Onda, Fausto Puntoriero, Sebastiano Campagna,* Yusuke Tamaki, and Osamu Ishitani*

Cite This: *ACS Catal.* 2023, 13, 9025−9032

Read Online

ACCESS | Metrics & More | Article Recommendations | Supporting Information

ABSTRACT: Supramolecular photocatalysts, wherein redox photosensitizer (PS) and catalyst (CAT) molecules are connected to each other, have been extensively studied because of their high photocatalytic activity in both homogeneous and heterogeneous environments compared with the corresponding mixed systems of separated PS and CAT. A supramolecular photocatalyst **RuC2Ph-C2Re**, wherein $[Ru(diimine)_3]^{2+}$ redox PS and *fac*-$[Re(diimine)(CO)_3\{OC(O)OCH_2CH_2N(CH_2CH_2OH)_2\}]$ CAT units were spatially separated by a bridging ligand $p(\text{-}C_2H_4)_2Ph$ consisting of 8 C−C bonds including a *p*-phenylene ring, was developed. Although the rate of intramolecular electron transfer of **RuC2PhC2Re** from one-electron-reduced Ru unit to the Re unit, which is a critical process of photocatalysis proceeding through the bond mechanism, was slower than that of **RuC2Re** having shorter bridging ligand with an ethylene chain, it could reduce CO_2 to CO with higher durability (TON = 3880) than **RuC2Re** (TON = 2800). These results clearly suggest that the PS and CAT units can be separated further without lowering photocatalysis of supramolecular photocatalysts because the rate of intramolecular electron transfer is much faster, even in **RuC2PhC2Re**, than that of the subsequent processes in photocatalytic CO_2 reduction.

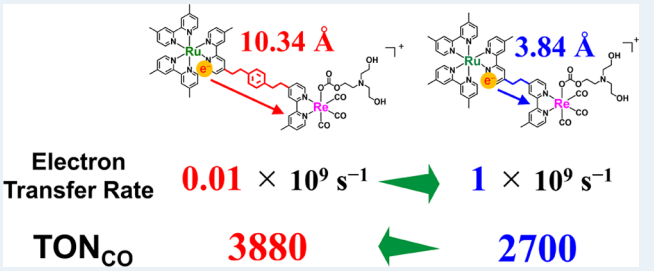

KEYWORDS: *photocatalytic CO_2 reduction, supramolecular photocatalyst, long-distance intermolecular electron transfer, time-resolved infrared spectroscopy, metal complex*

INTRODUCTION

Photocatalytic CO_2 reduction using sunlight has attracted attention as a prospective technology to solve both the global warming problem and depletion of energy and carbon resources. To develop efficient and durable molecular photocatalytic systems for CO_2 reduction, suitable combinations of two components are necessary: a redox photosensitizer (PS), which induces photochemical electron transfer from a reductant to another component, and a catalyst (CAT), which multiplies the accepted electrons from the PS and reduces CO_2 to multi-electron-reduced species, such as CO, HCOOH, and CH_4.[1,2]

Binuclear complexes with both the PS and CAT units connected to each other by a bridging ligand, called supramolecular photocatalysts, have been reported as single-molecule photocatalysts. Some of them exhibit much higher photocatalysis, i.e., higher efficiency and durability, compared with the mixture of the corresponding PS and CAT molecules with a single role owing to the rapid intramolecular electron transfer from the PS unit to the CAT unit without diffusion collision.[3−6] For achieving this advantage, supramolecular photocatalysts should fulfill the following conditions: (1) electron transfer must proceed from the one-electron-reduced PS unit to the CAT unit and (2) the reduction power of the CAT unit must not be lowered by connecting to the PS unit. For example, binuclear Ru(II)−Re(I) complexes, $[Ru(diimine)_3]^{2+}$ and $[Re(diimine)(CO)_3Cl]$ units connected with a bridging ligand conjugated with the diimine ligands showed much lower photocatalytic activity than a mixture of the corresponding mononuclear complexes because the conjugation lowers the π^* orbital energy of the diimine ligand of the CAT, which reduces the reduction power of the CAT.[3,7] Based on these molecular architectures, high-functioning supramolecular photocatalysts with an alkyl chain, typically $(-C_2H_4-)$, connecting the diimine ligands of the PS and CAT units have been developed. It has been reported that intramolecular electron transfer proceeds via a through-bond

Received: March 28, 2023
Revised: May 25, 2023
Published: June 23, 2023

https://doi.org/10.1021/acscatal.3c01407
ACS Catal. 2023, 13, 9025−9032

Chart 1. Structures of the Supramolecular Photocatalysts and Model Mononuclear Complexes

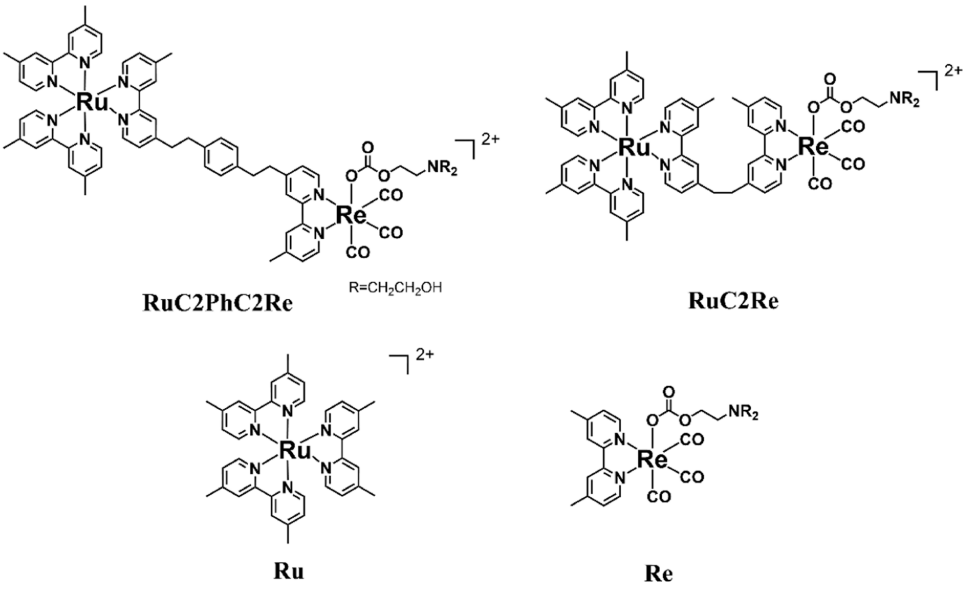

Scheme 1. Conceptual Images of a Hybrid Photocatalytic System with a Long Bridging Ligand

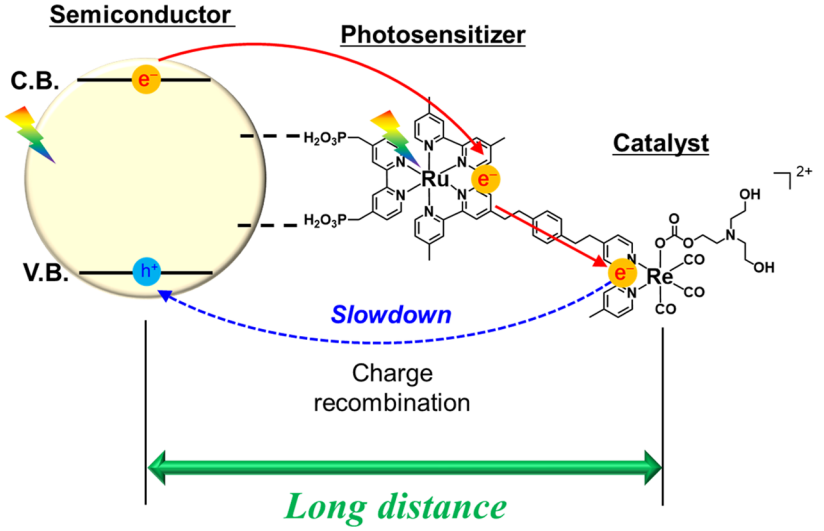

mechanism in these supramolecular photocatalysts.[8,9] Therefore, the rate of electron transfer decays exponentially with the length of the alkyl chain.

Although many efficient molecular photocatalytic systems, including supramolecular photocatalysts, for CO_2 reduction have been reported, one controversial point for the future practical application of photocatalytic CO_2 reduction is the use of water as a reductant for CO_2 reduction. From this viewpoint, the hybridization of supramolecular and semiconductor photocatalysts with high water oxidation power is a prospective candidate.[10−14] In these systems, according to the artificial Z-scheme, both the PS units of the supramolecular photocatalysts and semiconductor photocatalysts are excited to induce electron transfer from the reductant to the CAT units. Moreover, the supramolecular photocatalysts have an advantage over the mixed system of mononuclear PS and CAT because systems using mononuclear PS and CAT molecules cannot ensure efficient electron transfer from PS to CAT owing to the random fixation of PS and CAT. We first reported a hybrid system with Ag-loaded TaON particles as the semiconductor photocatalyst and Ru(II)−Ru(II) supramolecular photocatalyst connected with the methyl phosphonic groups of the diimine ligand of the PS unit.[11] The hybrid photocatalytic system has a much stronger oxidation power than the Ru(II)−Ru(II) supramolecular photocatalyst, wherein photocatalytic CO_2 reduction proceeds using methanol as a sacrificial electron donor that cannot be oxidized by the excited PS unit of the supramolecular photocatalyst. However, water cannot be used as an electron donor even though TaON has sufficient power to photochemically oxidize water to O_2.[15] A serious problem is the reoxidation of the reduced CAT unit by the oxidation sites of TaON because the CAT units are probably localized too close to the TaON surface. One of the solutions for reducing the possibility of this undesirable back-electron transfer process is to extend the distance between the CAT unit and semiconductor surface.

In this study, based on the investigation described above, we developed a new Ru(II)−Re(I) supramolecular photocatalyst, i.e., **RuC2PhC2Re** (Chart 1), wherein PS and CAT units are connected by a $p(\text{-}C_2H_4)_2Ph$ chain, which implies that these

https://doi.org/10.1021/acscatal.3c01407
ACS Catal. 2023, 13, 9025−9032

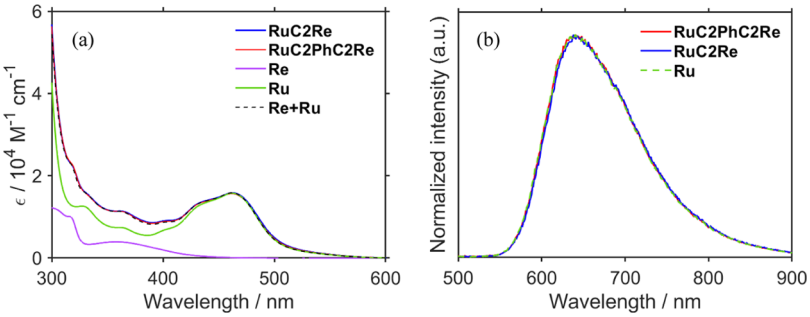

Figure 1. (a) UV−vis absorption spectra of **RuC2PhC2Re** (red), **RuC2Re** (blue), **Re** (purple), and **Ru** (green) and summation spectra of **Re** and **Ru** (black) in DMA−TEOA (5:1 v/v). (b) Emission spectra of **RuC2PhC2Re** (red), **RuC2Re** (blue), and **Ru** (green) in a CO_2-saturated DMA−TEOA (5:1 v/v); excitation wavelength: 460 nm.

units are separated by 8 carbon−carbon bonds. As this bridging ligand has a rigid *p*-phenylene ring between the PS and CAT units, the CAT unit can always be spatially separated from the PS unit, and should be directly connected to the semiconductor surface in the future (Scheme 1). The distance between the carbon at the 4-position of the bridging bipyridine moieties of the central Ru(II) and Re(I) complex units in **RuC2PhC2Re** (10.34 Å; Figure S8), which was calculated using density functional theory (DFT), is 2.7 times longer compared with that of another well-studied Ru(II)−Re(I) supramolecular photocatalyst with the same PS and CAT units connected to a shorter (−C_2H_4−) chain (**RuC2Re**, Scheme 1) (3.84 Å; Figure S9). Additionally, phenylene may promote through-bond electron transfer compared with the alkyl chain and prevent the intramolecular electron transfer rate from slowing down.[16] The photocatalysis activity of **RuC2PhC2Re** for CO_2 reduction was compared with that of **RuC2Re** in this study. The intramolecular electron transfer process from the reduced PS unit to the CAT unit in both supramolecular photocatalysts was determined by time-resolved infrared (TR-IR) measurements. Notably, in both supramolecular photocatalysts, the CAT unit is *fac*-[Re(BL)$(CO)_3${OC(O)-$OC_2H_4N(C_2H_4OH)$}] (BL = bridging ligand), where deprotonated triethanolamine (TEOA) captures CO_2 as a carbonate ester ligand. It has been reported that this type of Re(I) complex can efficiently catalyze CO_2 reduction to CO with high selectivity and durability.

RESULTS AND DISCUSSION

Synthesis and Photophysical Properties of RuC2Ph-C2Re. The new complexes, shown in Chart 1, were prepared from the corresponding chloro-rhenium derivatives, as described in the Experimental Section. The UV−vis absorption spectra of **RuC2PhC2Re**, **RuC2Re**, **Ru**, and **Re** are shown in Figure 1a; all of **RuC2PhC2Re**, **RuC2Re**, and **Ru** showed the characteristic absorption of ^{1}MLCT transition of Ru(II) complexes at λ_{max} = 462 nm in *N*,*N*-dimethylacetamide (DMA)−TEOA (5:1 v/v) mixed solutions. The similarity between the spectra of **RuC2PhC2Re** and **RuC2Re** and the sum of the spectra of **Ru** and **Re** indicate that the electronic properties of each unit of **RuC2PhC2Re** are similar to those of **RuC2Re**, and the electronic interactions between the Ru- and Re-complex units of these supramolecular photocatalysts are weak. **RuC2PhC2Re** exhibited phosphorescence from the ^{3}MLCT excited state of the Ru PS unit at λ_{max} = 641 nm (Figure 1b and Table 1). This emission spectrum is consistent with that of **Ru**. The emission spectrum of the ^{3}MLCT excited state of the Ru unit of **RuC2Re** was slightly red-shifted ($\Delta\lambda_{max}$ = 2−3 nm). Therefore, although the electronic interaction between the ^{3}MLCT excited Ru and Re units is weaker in **RuC2PhC2Re** than in **RuC2Re** because of the extended bridging ligand, the interaction is quite weak even in **RuC2Re**. These results indicate that the difference in the bridging ligands did not affect the electronic structures of the ground states and ^{3}MLCT excited states of these supramolecular photocatalysts.

Table 1. Photophysical Properties

	λ_{em}, nm[a]	τ, μs[b]	k_q[c], 10^8 M^{-1} s^{-1}	η_q[d]
RuC2PhC2Re	641	761 ± 1	10	0.99
RuC2Re	644	762 ± 1	10	0.99
Ru	640	748 ± 1		

[a]Measured in DMA−TEOA (5:1 v/v) at 25 °C. The samples were saturated with CO_2. Excitation wavelength: 460 nm. [b]Excitation wavelength: 510 nm. [c]Excitation wavelength: 520 nm. [d]Quenching fraction with 0.1 M BIH: $\eta_q = k_q\tau[BIH]/(1 + k_q\tau[BIH])$.

Photocatalytic Reactions. A DMA−TEOA (5:1 v/v) mixed solution (2 mL) containing **RuC2PhC2Re** (0.05 mM, 0.1 μmol) and BIH (0.1 M, 200 μmol) was irradiated at λ_{ex} = 490−620 nm (λ_{max} = 530 nm) using an LED light source under CO_2 atmosphere. CO was produced (183 μmol, TON = 1800 after 20 h) with high selectivity (>99%), and small amounts of HCOOH (1.2 μmol) and trace amounts of H_2 were detected (Figure 2a). BIH functioned as a two-electron donor in various photocatalytic reactions.[17] Therefore, a total TON > 1800 indicated that more than 90% of the added BIH was already consumed during the photocatalytic reaction for 20 h. Figure S6 shows the changes in the UV−vis absorption spectra of the reaction solution before and after the photocatalytic reaction. The broad absorption band at 400−480 nm, attributed to ^{1}MLCT transition, slowly decreased during the photocatalytic reaction, and a new band appeared at 480−620 nm as the irradiation time increased. These spectral changes indicate that part of the PS unit of **RuC2PhC2Re** changed its structure to the corresponding solvento Ru(II) complex via the dissociation of one of the diimine ligands.[18] Therefore, the primary reasons for the reduced photocatalytic activity are the consumption of BIH and decomposition of the PS unit. To avoid insufficient BIH during the photocatalytic reaction, the reaction was performed at a lower concentration of **RuC2PhC2Re** (0.01 mM). The TON_{CO} increased to 3880 ± 80 after 60 h irradiation (Table 2). The quantum yield of CO production was Φ_{CO} = 46%, measured using 480 nm monochromatic light (1.0×10^{-8} Einstein s^{-1}) (Figure S3a).

https://doi.org/10.1021/acscatal.3c01407
ACS Catal. 2023, 13, 9025−9032

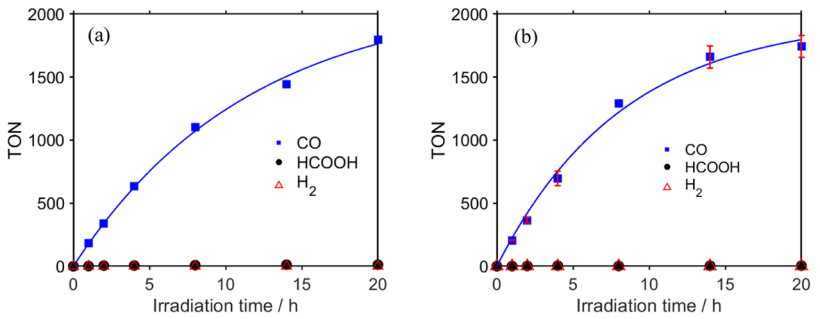

Figure 2. Photocatalytic formation of CO (blue), H_2 (red), and formic acid (black). CO_2-saturated DMA−TEOA (5:1 v/v) solutions containing (a) **RuC2PhC2Re** (0.05 mM) or (b) **RuC2Re** (0.05 mM) as a photocatalyst and BIH (0.1 M) as a sacrificial electron donor were irradiated at λ_{ex} = 490−620 nm (λ_{max} = 530 nm). The error bars were obtained using the results of two independent experiments.

Table 2. Photocatalysis of RuC2PhC2Re and RuC2Re

			products, μmol (TON)[b]			
entry	complex	time[a], h	CO	HCOOH	H_2	Φ_{CO}[c], %
1[d]	**RuC2PhC2Re**	1	18.6 (183)	0.1 (1)	ND[g]	46
		20	183 (1800)	1.2 (12)	trace	
2[d]	**RuC2Re**	1	20.1 ± 0.5 (206 ± 1)	0.2 (2)	ND[g]	40
		20	175 ± 8 (1740 ± 90)	0.7 ± 0.1 (7 ± 1)	trace	
3[e]	**RuC2PhC2Re**	60	79 ± 2 (3880 ± 80)	5.7 ± 0.2 (280 ± 10)	trace	
4[e]	**RuC2Re**	60	55 ± 6 (2700 ± 300)	1.3 ± 0.7 (70 ± 30)	trace	
5[f]	**Ru + Re**	60	45 ± 3 (2260 ± 150)	2.7 ± 0.1 (137 ± 4)	trace	

[a]Irradiation time. [b]DMA−TEOA (5:1 v/v, 2 mL) solutions containing the photocatalyst and BIH (0.1 M) were irradiated using 490−620 nm LED light (λ_{max} = 530 nm). [c]DMA−TEOA (5:1 v/v, 4 mL) solutions containing the photocatalyst and BIH (0.1 M) were irradiated at λ_{ex} = 480 nm (light intensity: 1.0×10^{-8} Einstein s^{-1}). [d]Concentration of the complex was 0.05 mM. [e]Concentration of the complex was 0.01 mM. [f]DMA−TEOA (5:1 v/v, 2 mL) solutions containing **Ru** (0.01 mM), **Re** (0.01 mM), and BIH (0.1 M) were irradiated using 490−620 nm LED light (λ_{max} = 530 nm). [g]Not detected.

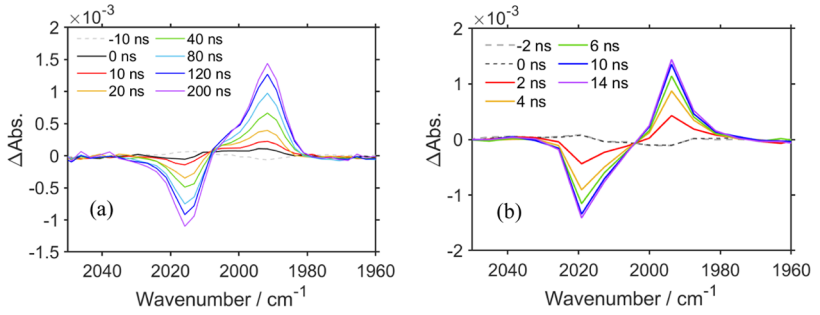

Figure 3. TR-IR spectra measured at various time delays after pulse excitation. (a) DMA−TEOA (5:1 v/v) mixed solution containing **RuC2PhC2Re** (0.2 mM) and BIH (0.3 M) was irradiated using 526.5 nm laser light (25 Hz) and probed (50 Hz). (b) DMF-TEOA (5:1 v/v) mixed solution containing **RuC2Re** (0.2 mM) and BIH (0.3 M) was irradiated using 532 nm pump light (500 Hz) and probed (1000 Hz).

The reported Ru(II)−Re(I) supramolecular photocatalyst **RuC2Re** with the Ru PS and Re CAT units connected to an ethylene chain (Chart 1), which is a much shorter bridging ligand than that in **RuC2PhC2Re**, has been well studied as a photocatalyst for CO_2 reduction. Photocatalytic reaction experiments under the same reaction conditions using **RuC2Re** instead of **RuC2PhC2Re** as the photocatalyst were performed for comparison with **RuC2PhC2Re** (Figure 1 and Table 1). At a higher concentration of the photocatalyst (0.05 mM), both photocatalysts exhibited comparable durability, selectivity (>99%), and initial rates of CO production (Figure 1). However, at a lower concentration of the photocatalyst, the durability of **RuC2PhC2Re** was clearly higher (TON_{CO} = 3880 ± 80) than that of **RuC2Re** (TON_{CO} = 2700 ± 300). We cannot clarify the reason(s) why **RuC2PhC2Re** showed higher durability in the photocatalytic reaction conditions compared to that of **RuC2Re**, yet. The structure change of the Ru photosensitizer unit of **RuC2PhC2Re** to the solvento complex was slightly slower than that of **RuC2Re**, especially in the initial stage of the photocatalytic reactions such as after 1 h irradiation in Figure S6. This means that this ligand substitution reaction, which proceeds via excitation of the one-electron reduced Ru complex unit, occurred slightly but more slowly in the photocatalytic system using **RuC2PhC2Re** than that using **RuC2Re**. A slightly higher quantum yield of CO was obtained in the photocatalytic system using **RuC2PhC2Re** (Φ_{CO} = 46%) compared with **RuC2Re** (Φ_{CO} = 40%) (Figure S3b).

Intramolecular Electron Transfer. The excited Ru units were reductively quenched by BIH (Figures S4 and S5). The quenching rate constants (k_q) of **RuC2PhC2Re** and **RuC2Re** obtained by Stern−Volmer plots had nearly the same values

https://doi.org/10.1021/acscatal.3c01407
ACS Catal. 2023, 13, 9025−9032

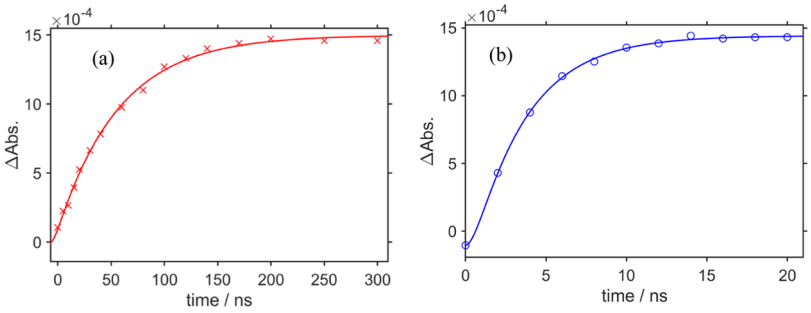

Figure 4. Changes of ΔAbs at (red) 1992 cm^{-1} shown in Figure 3a and (blue) 1994 cm^{-1} in Figure 3b and their fitting (see the Supporting Information).

(1.0×10^9 M^{-1} s^{-1}); the quenching fractions were 0.99 ([BIH] = 0.1 M) in both the cases (Table 1). Because the emission lifetimes of **RuC2PhC2Re** (761 μs) and **RuC2Re** (762 μs) were close to that of **Ru** (748 μs) (Table 1), the intramolecular electron transfer from the excited Ru unit to the Re unit (i.e., oxidative quenching) was negligible for both **RuC2PhC2Re** and **RuC2Re**. These results indicate that the photocatalytic reactions should be initiated by reductive quenching of the excited Ru unit by BIH in both the systems.

TR-IR measurements of a CO_2 saturated DMA−TEOA (5:1 v/v) solution containing **RuC2PhC2Re** (0.2 mM) and BIH (0.3 M) were performed using the pump−probe method via a nanosecond laser pump pulse (526.5 nm) and an ultrafast infrared pulse generated from the output of a Ti:sapphire amplifier as the probe pulse. The FT-IR spectra of **RuC2PhC2Re** and **RuC2Re** show an absorption band attributed to the symmetric vibration of the CO ligands at ν_{CO} = 2019 cm^{-1} (Figure S7). Figure 3a shows TR-IR spectral changes of **RuC2PhC2Re** at 1960−2050 cm^{-1} after the excitation; a bleaching band at 2016 cm^{-1} and positive peak at 1992 cm^{-1} appeared after the excitation. The positive peak is attributed to one-electron reduced species (OERS) of the Re unit of **RuC2PhC2Re**, i.e., **RuC2PhC2(Re)**$^-$, which should be produced by reductive quenching of the excited state of the Ru unit followed by intramolecular electron transfer from the Ru unit to the Re unit (eqs 1 and 2).[8,9,19] Using **RuC2Re**, similar spectral changes were observed, as shown in Figure 3b; the bleaching band at 2019 cm^{-1} and positive peak at 1994 cm^{-1} assigned to **RuC2(Re)**$^-$ appeared after the excitation (λ_{ex} = 532 nm) in DMF-TEOA (5:1 v/v).

$$^3(Ru)^* - BL - Re + BIH \rightarrow (Ru)^- - BL - Re + BIH^{\bullet +} \quad (1)$$

$$(Ru)^- - BL - Re \leftrightharpoons Ru - BL - (Re)^- \quad (2)$$

However, the rates of intramolecular electron transfer from the OERS of the Ru PS unit, which was produced by reductive quenching with BIH, to the Re unit were significantly different between the systems using **RuC2PhC2Re** and **RuC2Re** (Figure 4). The observed production rate constants of OERS of the Re unit, i.e., **RuC2PhC2(Re)**$^-$ and **RuC2(Re)**$^-$, were determined as $k_{obs} = 1.7 \times 10^7$ and 2.9×10^8 s^{-1}, respectively, using a single exponential function. Notably, the intramolecular electron transfer reactions were reversible. In other words, k_{obs} includes the kinetics of the reductive quenching process and both forward and backward electron transfer processes. The forward and backward electron transfer rates were estimated using the equilibrium constants for the reversible reaction calculated from the driving forces (ΔG_{et} = −0.03 eV) of the forward reaction; ΔG_{et} was estimated from the reported reduction potentials of the mononuclear Ru and Re complexes (Table 3 and Figure 4; see the Supporting Information).[19] As reported, in the case of **RuC2Re**, the intramolecular electron transfer proceeds via a through-bond mechanism.[9] Therefore, the difference in the rates of intramolecular electron transfer between the OERSs of **RuC2PhC2Re** and **RuC2Re** seems reasonable because the bridging carbon chain is elongated from C_2 (**RuC2Re**) to C_8 (**RuC2PhC2Re**), which slows down the electron transfer rate. Notably, the photocatalytic activity of **RuC2PhC2Re** is higher than that of **RuC2Re**, although the intramolecular electron transfer, which is a critical process in photocatalytic reactions, is 2 orders of magnitude slower. This indicates that the intramolecular electron transfer process is not the rate-determining process in the photocatalytic reactions using **RuC2PhC2Re** and **RuC2Re**. We recently reported that the rate of the subsequent process of **RuC2(Re)**$^-$ in the photocatalytic reaction, giving an intermediate whose structure is still unknown, is 1.8 s^{-1} in DMSO-TEOA (5:1 v/v) that is 7 orders of magnitude slower than the intramolecular electron transfer rate.[19] The rate of the intramolecular electron transfer in the case of **RuC2PhC2Re** should be much faster than that of the subsequent process of **RuC2PhC2(Re)**$^-$ because of the similarity of the properties of the Re CAT unit between **RuC2Re** and **RuC2PhC2Re**. In other words, the distance between the Ru and Re units in supramolecular photocatalysts can be extended considerably using not only an alkyl chain but also an aromatic group or group without losing photocatalytic activity.

Table 3. Rate Constants of Forward and Backward Intramolecular Electron Transfer

	k_{et}, 10^9 s^{-1}	k_{bet}, 10^9 s^{-1}
RuC2PhC2Re	0.01	0.004
RuC2Re	1	0.4

EXPERIMENTAL SECTION

General Procedures. DMA was dried on 4 Å molecular sieves at room temperature and distilled at reduced pressure before use. The TEOA was distilled under reduced pressure (<133 Pa). The distilled solvents were stored under an Ar atmosphere. All other reagents were of reagent grade and used without further purification. The UV−vis absorption spectra were measured using a JASCO V-670 spectrophotometer. FT-IR spectra were recorded on a JASCO FT-IR 6600 spectrophotometer. The emission spectra were measured

https://doi.org/10.1021/acscatal.3c01407
ACS Catal. 2023, 13, 9025−9032

using HORIBA Fluorolog-3 and Fluorolog-NIR spectrofluorometers. The emission lifetimes were measured using the HORIBA Jobin-Yvon FluoroCube time-correlated single-photon counting system. The samples used for the emission spectra and lifetime measurements were saturated with CO_2.

Synthesis. BIH and *fac*-[$(dmb)_2$Ru(bpyC2bpy)Re$(CO)_3$MeCN]$(PF_6)_3$ (**RuC2Re(MeCN)**, dmb = 4,4′-dimethyl-2,2′-bipyridine, **bpyC2bpy** = (4′-methyl-[2,2′-bipyridine]-4-yl)-CH_2CH_2-(4′-methyl-[2,2′-bipyridine]-4-yl)) were synthesized according to the procedures reported in the literature.[20−22] **bpyC2PhC2bpy** = (1,4-Bis[2-(4′-methyl-2,2′-bipyridyl-4-yl)ethyl]benzene) and *fac*-[$(dmb)_2$Ru(bpyC2PhC2bpy)]$(PF_6)_2$ (**RubpyC2PhC2bpy**) were prepared by modifying synthetic strategies reported in the literature.[23]

bpyC2PhC2bpy. 4,4′-Dimethyl-2,2′-dipyridyl (1.88 g, 10 mmol) was dissolved in 140 mL of dry THF under an Ar atmosphere. The solution was cooled at −33 °C, and the 1 M solution of lithium diisopropylamide (12 mmol, 12 mL) was added dropwise. After stirring for 90 min, 50 mL of a 1,4-Bis(bromomethyl)benzene (1.09 g, 4.1 mmol) solution was added dropwise, and it was stirred for 48 h. The reaction was quenched by adding 20 mL of water. Subsequently, the mixture was extracted with diethyl ether (3 × 250 mL) and dichloromethane (2 × 100 mL). The organic phase was dried over sodium sulfate anhydrous. The pale pink residue was recrystallized from ethanol to yield a pure white solid. Yield: 1.00 g, 52%. ^{1}H NMR (500 MHz, 25 °C, CD_2Cl_2) δ = 8.51 (t br, 4H), 8.31−8.28 (d, 4H), 7.14 (m, 6H), 7.11 (d, 2H), 2.99 (s, 8H), and 2.45 (s, 6H). ^{13}C NMR (126 MHz, 25 °C, CD_2Cl_2) δ = 156.08, 155.88, 151.55, 148.88, 148.77, 148.05, 138.88, 128.41, 124.56, 123.87, 121.64, 120.95, 37.32, 36.19, and 20.86. Elemental analysis Calc. for $C_{32}H_{30}N_4$: C, 81.67; H, 6.43; N, 11.91; Elemental analysis Found: C, 81.59; H, 6.49; N, 11.88.

RubpyC2PhC2bpy. **bpyC2PhC2bpy** (200 mg, 0.42 mmol) was dissolved in 25 mL of a mixture of 1,2-dichloroethane/ethanol (1:1 v/v) under an Ar atmosphere. *cis*-[$Ru(dmb)_2Cl_2$]$2H_2O$ (65 mg, 0.12 mmol) was dissolved in 10 mL of the same solvent mixture and slowly added dropwise to the reaction mixture at reflux. The solution was refluxed for 2 h. The crude product was dissolved in distilled water, and the unreacted ligand was filtered. The product was isolated as an orange solid by adding NH_4PF_6 and washing with cold water. Yield: 128 mg, 86.7%. Elemental analysis Calc. for $C_{56}H_{54}F_{12}N_8P_2Ru$: C, 54.68; H, 4.42; N, 9.11; Elemental analysis Found: C, 54.72; H, 4.45; N, 9.09.

*fac-[$(dmb)_2$Ru(bpyC2PhC2bpy)Re$(CO)_3$Cl]$(PF_6)_2$ (**RuC2PhC2Re(Cl)**).* RuL2 (38 mg, 0.037 mmol) was dissolved in 18 mL of a mixture of 1,2-dichloroethane and toluene (1:1, v/v), and it was refluxed under an Ar atmosphere. Re$(CO)_5$Cl (24 mg, 0.066 mmol) was dissolved in 5 mL of the same solvent, and the solution was stirred for 4 h under Ar atmosphere. Subsequently, the product was evaporated under vacuum. The crude product was dissolved in ethanol, precipitated by adding excess NH_4PF_6, filtered, and washed several times with diethyl ether. Flash chromatography on a Sephadex G-15 column (eluent: ethanol) was used for further purification. Yield: 46 mg, 80.8%. Elemental analysis Calc. for $C_{59}H_{54}ClF_{12}N_8O_3P_2ReRu$: C, 46.14; H, 3.54; N, 7.30; Elemental analysis Found: C, 46.19; H, 3.58; N, 7.28.

*fac-[$(dmb)_2$Ru(bpyC2PhC2bpy)Re$(CO)_3$MeCN]$(PF_6)_3$ (**RuC2PhC2Re(MeCN)**).* A MeCN solution (40 mL) containing **RuC2PhC2Re(Cl)** (24 mg, 0.016 mol) and aqueous solution (10 mL) containing an excess amount of NH_4PF_6 (1.15 g) were mixed and stirred at 50 °C for 15 h. After removing the solvent by evaporation, the crude product was purified by ion-exchange column chromatography using a CM-Sephadex C25 column (eluent: H_2O−MeCN (1:1 v/v) containing NH_4PF_6). Following the evaporation of MeCN, the residue was extracted from the aqueous suspension with CH_2Cl_2 and the organic phase was dried over $MgSO_4$. After the solvent was evaporated, the resulting red solid was purified by recrystallization from CH_2Cl_2/Et_2O to obtain a red-orange powder. Yield: 4.1 mg, 15%. ^{1}H NMR (400 MHz, CD_3CN): δ/ppm = 8.82 (dd, 2H, J = 5.2, 1.4 Hz, α-py3), 8.32−8.29 (m, 8H, γ-py-3, α-py-6, β-py-3, δ-py3), 7.53−7.46 (m, 8H, γ-py-6, α-py-5, β-py-6, δ-py-6), 7.20−7.15 (m, 10H, β-py-5, γ-py-5, δ-py-5, -C_6H_4-), 3.12−2.90 (m, 8H, −CH_2CH_2−), 2.57 (s, 3H, α-py-CH_3), 2.50 (s, 15 H, β-py-CH_3, γ-py-CH_3, δ-py-CH_3), and 2.03 (s, 3H, CH_3CN−) (Figure S1).

RuC2PhC2Re. **RuC2PhC2Re(MeCN)** was dissolved in DMA, and the resulting solution was kept at room temperature in the dark under an Ar atmosphere for longer than 7 h to change the MeCN ligand of all of the added Re complexes to DMA; subsequently, TEOA was added into the solution (DMA:TEOA = 5:1 v/v), which was kept under an Ar atmosphere in the dark at room temperature for longer than 3 h. The solution was bubbled with CO_2 to obtain a DMA−TEOA (5:1 v/v) solution containing **RuC2PhC2Re**. The formation of **RuC2PhC2Re** was confirmed by FT-IR spectroscopy (Figure S7).

RuC2Re. **RuC2Re** was synthesized from **RuC2Re(MeCN)** by the same procedure as **RuC2PhC2Re**.

Photocatalytic Reactions. To measure the TON, DMA−TEOA (5:1 v/v, 2 mL) solutions containing the photocatalyst and BIH (0.1 M) in Pyrex test tubes (11 mL volume) were purged with CO_2 for 30 min and subsequently irradiated at 490−620 nm (λ_{max} = 530 nm) using the Iris-MG merry-go-round irradiation apparatus with an LED light source (CELL System Co.). To carry out quantum yield measurements, a CO_2-saturated DMA−TEOA (5:1 v/v, 4 mL) solution containing complex (0.05 mM) and BIH (0.1 M) in an 11 mL necked quartz cubic cell (path length: 1 cm) was irradiated at λ_{ex} = 480 nm (1.0×10^{-8} Einstein s^{-1}) using a 300 W Xe lamp (Asahi Spectra MAX-303) equipped with a bandpass filter in the Shimadzu QYM-01 photoreaction quantum yield evaluation system. The sample temperature was kept at 25 ± 0.1 °C using an EYELA NCB-1210 temperature bath. The gaseous products, i.e., CO and H_2, and formic acid in the solution were analyzed using gas chromatography with a TCD detector (GL Science GC323) and capillary electrophoresis system (Agilent Technology 7100L), respectively.

TR-IR Measurement. TR-IR spectroscopic measurements were performed using the pump−probe method with a subnanosecond laser for the pump pulse and femtosecond Ti:sapphire laser for the probe pulse, as reported in the literature,[24−26] and the details are described in the Supporting Information.

DFT Calculation. Quantum chemical calculations based on DFT were performed using the Gaussian 16 package.[27] Geometry optimization was performed in DMA (ε = 37.8) using ωB97XD function, LanL2DZ basis set for Re with an added f polarization function,[28] and 6-311G+(d,p) for the other elements.

https://doi.org/10.1021/acscatal.3c01407
ACS Catal. 2023, 13, 9025−9032

CONCLUSIONS

We successfully synthesized a new efficient supramolecular photocatalyst (**RuC2PhC2Re**) for CO_2 reduction, wherein a Ru(II) photosensitizer unit and Re(I) catalyst unit were separated by eight carbon−carbon bonds, including a *p*-phenylene ring. Although the intramolecular electron transfer rate from the reduced Ru unit to the catalyst unit in **RuC2PhC2Re** was slower than that in **RuC2Re**, wherein the Ru and Re units were connected by a much shorter ethylene chain, it was much faster (7 orders of magnitude) than the subsequent process of CO_2 reduction. The durability of **RuC2PhC2Re** was higher than that of **RuC2Re**. These results suggest that a greater extension of the distance between the photosensitizer and catalyst units in supramolecular photocatalysts is possible without a decrease in the photocatalysis for CO_2 reduction. Therefore, in hybrid photocatalytic systems with solid materials, such as semiconductor photocatalysts, the catalyst unit can be separated far away from the semiconductor surface without loss of photocatalytic activity. This strategy should be applicable for various redox photocatalysts consisting of different oxidation and reduction sites that should be separated from each other for achieving efficient photocatalysis not only for CO_2 reduction but also for other targets such as water splitting and organic synthesis.

ASSOCIATED CONTENT

Supporting Information

The Supporting Information is available free of charge at https://pubs.acs.org/doi/10.1021/acscatal.3c01407.

NMR spectra, redox properties, quantum yield measurements, quenching experiments, UV−vis absorption spectral changes during the photocatalytic reactions, FT-IR spectra before and after the CO_2 capture reaction, kinetic analysis of intramolecular electron transfer, optimized structure calculated by the DFT method, and experimental details of the TR-IR measurements (PDF)

AUTHOR INFORMATION

Corresponding Authors

Sebastiano Campagna − *Dipartimento di Scienze Chimiche, Biologiche, Farmaceutiche ed Ambientali, Centro di Ricerca Interuniversitario per la Conversione Chimica dell'energia Solare (SOLAR-CHEM, Sezione di Messina), Università di Messina, 98166 Messina, Italy;* orcid.org/0000-0003-3385-2528; Email: campagna@unime.it

Osamu Ishitani − *Department of Chemistry, School of Science, Tokyo Institute of Technology, Tokyo 152-8550, Japan; Department of Chemistry, Graduate School of Advanced Science and Engineering, Hiroshima University, Higashi-Hiroshima, Hiroshima 739-8526, Japan;* orcid.org/0000-0001-9557-7854; Email: ishitani@chem.titech.ac.jp

Authors

Kei Kamogawa − *Department of Chemistry, School of Science, Tokyo Institute of Technology, Tokyo 152-8550, Japan*

Antonio Santoro − *Dipartimento di Scienze Chimiche, Biologiche, Farmaceutiche ed Ambientali, Centro di Ricerca Interuniversitario per la Conversione Chimica dell'energia Solare (SOLAR-CHEM, Sezione di Messina), Università di Messina, 98166 Messina, Italy*

Ambra M. Cancelliere − *Dipartimento di Scienze Chimiche, Biologiche, Farmaceutiche ed Ambientali, Centro di Ricerca Interuniversitario per la Conversione Chimica dell'energia Solare (SOLAR-CHEM, Sezione di Messina), Università di Messina, 98166 Messina, Italy*

Yuushi Shimoda − *Department of Chemistry, Graduate School of Science, Kyushu University, Fukuoka 819-0395, Japan*

Kiyoshi Miyata − *Department of Chemistry, Graduate School of Science, Kyushu University, Fukuoka 819-0395, Japan;* orcid.org/0000-0001-6748-1337

Ken Onda − *Department of Chemistry, Graduate School of Science, Kyushu University, Fukuoka 819-0395, Japan;* orcid.org/0000-0003-1724-2009

Fausto Puntoriero − *Dipartimento di Scienze Chimiche, Biologiche, Farmaceutiche ed Ambientali, Centro di Ricerca Interuniversitario per la Conversione Chimica dell'energia Solare (SOLAR-CHEM, Sezione di Messina), Università di Messina, 98166 Messina, Italy*

Yusuke Tamaki − *Department of Chemistry, School of Science, Tokyo Institute of Technology, Tokyo 152-8550, Japan;* orcid.org/0000-0003-4432-0025

Complete contact information is available at: https://pubs.acs.org/10.1021/acscatal.3c01407

Notes

The authors declare no competing financial interest.

ACKNOWLEDGMENTS

This work was funded in part by grants from the Italian Ministry of Foreign Affairs and International Cooperation (PGR project on Artificial Photosynthesis, collaboration Italy−Japan) and MUR-PNRR Samothrace Project. This work was also supported by JSPS KAKENHI, Grant Numbers JP22K19081 and JP20H00396. K.K. wishes to acknowledge the support from JSPS Fellowship for Young Scientists (JP22J21126). DFT calculations were performed on a TSUBAME3.0 supercomputer at the Tokyo Institute of Technology, supported by the MEXT Project of the Tokyo Tech Academy for Convergence of Materials and Informatics (TAC-MI).

REFERENCES

(1) Yamazaki, Y.; Takeda, H.; Ishitani, O. Photocatalytic reduction of CO_2 using metal complexes. *J. Photochem. Photobiol. C* **2015**, *25*, 106−137.

(2) Boutin, E.; Merakeb, L.; Ma, B.; Boudy, B.; Wang, M.; Bonin, J.; Anxolabéhère-Mallart, E.; Robert, M. Molecular catalysis of CO_2 reduction: recent advances and perspectives in electrochemical and light-driven processes with selected Fe, Ni and Co aza macrocyclic and polypyridine complexes. *Chem. Soc. Rev.* **2020**, *49*, 5772−5809.

(3) Gholamkhass, B.; Mametsuka, H.; Koike, K.; Tanabe, T.; Furue, M.; Ishitani, O. Architecture of Supramolecular Metal Complexes for Photocatalytic CO_2 Reduction: Ruthenium−Rhenium Bi- and Tetranuclear Complexes. *Inorg. Chem.* **2005**, *44*, 2326−2336.

(4) Tamaki, Y.; Ishitani, O. Supramolecular Photocatalysts for the Reduction of CO_2. *ACS Catal.* **2017**, *7*, 3394−3409.

(5) Nakajima, T.; Tamaki, Y.; Ueno, K.; Kato, E.; Nishikawa, T.; Ohkubo, K.; Yamazaki, Y.; Morimoto, T.; Ishitani, O. Photocatalytic Reduction of Low Concentration of CO_2. *J. Am. Chem. Soc.* **2016**, *138*, 13818−13821.

(6) Cancelliere, A. M.; Puntoriero, F.; Serroni, S.; Campagna, S.; Tamaki, Y.; Saito, D.; Ishitani, O. Efficient trinuclear Ru(II)-Re(I) supramolecular photocatalysts for CO_2 reduction based on a new tris-

chelating bridging ligand built around a central aromatic ring. *Chem. Sci.* **2020**, *11*, 1556−1563.
(7) Bian, Z.-Y.; Wang, H.; Fu, W.-F.; Li, L.; Ding, A.-Z. Two bifunctional RuII/ReI photocatalysts for CO_2 reduction: A spectroscopic, photocatalytic, and computational study. *Polyhedron* **2012**, *32*, 78−85.
(8) Koike, K.; Grills, D. C.; Tamaki, Y.; Fujita, E.; Okubo, K.; Yamazaki, Y.; Saigo, M.; Mukuta, T.; Onda, K.; Ishitani, O. Investigation of excited state, reductive quenching, and intramolecular electron transfer of Ru(II)-Re(I) supramolecular photocatalysts for CO_2 reduction using time-resolved IR measurements. *Chem. Sci.* **2018**, *9*, 2961−2974.
(9) Yamazaki, Y.; Ohkubo, K.; Saito, D.; Yatsu, T.; Tamaki, Y.; Tanaka, S.; Koike, K.; Onda, K.; Ishitani, O. Kinetics and Mechanism of Intramolecular Electron Transfer in Ru(II)-Re(I) Supramolecular CO_2-Reduction Photocatalysts: Effects of Bridging Ligands. *Inorg. Chem.* **2019**, *58*, 11480−11492.
(10) Sekizawa, K.; Maeda, K.; Domen, K.; Koike, K.; Ishitani, O. Artificial Z-Scheme Constructed with a Supramolecular Metal Complex and Semiconductor for the Photocatalytic Reduction of CO_2. *J. Am. Chem. Soc.* **2013**, *135*, 4596−4599.
(11) Kumagai, H.; Tamaki, Y.; Ishitani, O. Photocatalytic Systems for CO_2 Reduction: Metal-Complex Photocatalysts and Their Hybrids with Photofunctional Solid Materials. *Acc. Chem. Res.* **2022**, *55*, 978−990.
(12) Wada, K.; Eguchi, M.; Ishitani, O.; Maeda, K. Activation of the Carbon Nitride Surface by Silica in a CO-Evolving Hybrid Photocatalyst. *ChemSusChem* **2017**, *10*, 287−295.
(13) Wada, K.; Ranasinghe, C. S. K.; Kuriki, R.; Yamakata, A.; Ishitani, O.; Maeda, K. Interfacial Manipulation by Rutile TiO_2 Nanoparticles to Boost CO_2 Reduction into CO on a Metal-Complex/Semiconductor Hybrid Photocatalyst. *ACS Appl. Mater. Interfaces* **2017**, *9*, 23869−23877.
(14) Shizuno, M.; Kato, K.; Nishioka, S.; Kanazawa, T.; Saito, D.; Nozawa, S.; Yamakata, A.; Ishitani, O.; Maeda, K. Effects of a Nanoparticulate TiO_2 Modifier on the Visible-Light CO_2 Reduction Performance of a Metal-Complex/Semiconductor Hybrid Photocatalyst. *ACS Appl. Energy Mater.* **2022**, *5*, 9479−9486.
(15) Hitoki, G.; Takata, T.; Kondo, J. N.; Hara, M.; Kobayashi, H.; Domen, K. An oxynitride, TaON, as an efficient water oxidation photocatalyst under visible light irradiation ($\lambda \leq 500$ nm). *Chem. Commun.* **2002**, *16*, 1698−1699.
(16) Wenger, O. S.; Leigh, B. S.; Villahermosa, R. M.; Gray, H. B.; Winkler, J. R. Electron Tunneling Through Organic Molecules in Frozen Glasses. *Science* **2005**, *307*, 99−102.
(17) Tamaki, Y.; Koike, K.; Morimoto, T.; Ishitani, O. Substantial improvement in the efficiency and durability of a photocatalyst for carbon dioxide reduction using a benzoimidazole derivative as an electron donor. *J. Catal.* **2013**, *304*, 22−28.
(18) Lehn, J.-M.; Ziessel, R. Photochemical reduction of carbon dioxide to formate catalyzed by 2,2′-bipyridine- or 1,10-phenanthroline-ruthenium(II) complexes. *J. Organomet. Chem.* **1990**, *382*, 157−173.
(19) Kamogawa, K.; Shimoda, Y.; Miyata, K.; Onda, K.; Yamazaki, Y.; Tamaki, Y.; Ishitani, O. Mechanistic study of photocatalytic CO2 reduction using a Ru(ii)−Re(i) supramolecular photocatalyst. *Chem. Sci.* **2021**, *12*, 9682−9693.
(20) Ohkubo, K.; Yamazaki, Y.; Nakashima, T.; Tamaki, Y.; Koike, K.; Ishitani, O. Photocatalyses of Ru(II)−Re(I) binuclear complexes connected through two ethylene chains for CO_2 reduction. *J. Catal.* **2016**, *343*, 278−289.
(21) Hasegawa, E.; Seida, T.; Chiba, N.; Takahashi, T.; Ikeda, H. Contrastive photoreduction pathways of benzophenones governed by regiospecific deprotonation of imidazoline radical cations and additive effects. *J. Org. Chem.* **2005**, *70*, 9632−9635.
(22) Zhu, X. Q.; Zhang, M. T.; Yu, A.; Wang, C. H.; Cheng, J. P. Hydride, hydrogen atom, proton, and electron transfer driving forces of various five-membered heterocyclic organic hydrides and their reaction intermediates in acetonitrile. *J. Am. Chem. Soc.* **2008**, *130*, 2501−2516.
(23) Schmehl, R. H.; Auerbach, R. A.; Wacholtz, W. F.; Elliott, C. M.; Freitag, R. A.; Merkert, J. W. Formation and photophysical properties of iron-ruthenium tetranuclear bipyridyl complexes of the type {[(bpy)2Ru(L-L)]3Fe}. *Inorg. Chem.* **1986**, *25*, 2440−2445.
(24) Mukuta, T.; Fukazawa, N.; Murata, K.; Inagaki, A.; Akita, M.; Tanaka, S. I.; Koshihara, S.-Y.; Onda, K. Infrared Vibrational Spectroscopy of $[Ru(bpy)_2(bpm)]^{2+}$ and $[Ru(bpy)_3]^{2+}$ in the Excited Triplet State. *Inorg. Chem.* **2014**, *53*, 2481−2490.
(25) Mukuta, T.; Simpson, P. V.; Vaughan, J. G.; Skelton, B. W.; Stagni, S.; Massi, M.; Koike, K.; Ishitani, O.; Onda, K. Photochemical Processes in a Rhenium(I) Tricarbonyl N-Heterocyclic Carbene Complex Studied by Time-Resolved Measurements. *Inorg. Chem.* **2017**, *56*, 3404−3413.
(26) Mukuta, T.; Tanaka, S. I.; Inagaki, A.; Koshihara, S.-Y.; Onda, K. Direct Observation of the Triplet Metal-Centered State in $[Ru(bpy)_3]^{2+}$ Using Time-Resolved Infrared Spectroscopy. *ChemistrySelect* **2016**, *1*, 2802−2807.
(27) Frisch, M. J.; Trucks, G. W.; Schlegel, H. B.; Scuseria, G. E.; Robb, M. A.; Cheeseman, J. R.; Scalmani, G.; Barone, V.; Petersson, G. A.; Nakatsuji, H.; Li, X.; Caricato, M.; Marenich, A. V.; Bloino, J.; Janesko, B. G.; Gomperts, R.; Mennucci, B.; Hratchian, H. P.; Ortiz, J. V.; Izmaylov, A. F.; Sonnenberg, J. L.; Williams, F.; Ding, F.; Lipparini, F.; Egidi, J.; Goings, B.; Peng, A.; Petrone, T.; Henderson, D.; Ranasinghe, V. G.; Zakrzewski, J.; Gao, N.; Rega, G.; Zheng, W.; Liang, M.; Hada, M.; Ehara, K.; Toyota, R.; Fukuda, J.; Hasegawa, M.; Ishida, T.; Nakajima, Y.; Honda, O.; Kitao, H.; Nakai, T.; Vreven, K.; Throssell, J. A.; Montgomery, A., Jr.; Peralta, J. E.; Ogliaro, F.; Bearpark, M. J.; Heyd, J. J.; Brothers, E. N.; Kudin, K. N.; Staroverov, V. N.; Keith, T. A.; Kobayashi, R.; Normand, J.; Raghavachari, K.; Rendell, A. P.; Burant, J. C.; Iyengar, S. S.; Tomasi, J.; Cossi, M.; Millam, J. M.; Klene, M.; Adamo, C.; Cammi, R.; Ochterski, J. W.; Martin, R. L.; Morokuma, K.; Farkas, O.; Foresman, J. B.; Fox, D. J. *Gaussian 16*, revision C.01; Gaussian, Inc.: Wallingford, CT, 2016.
(28) Ehlers, A. W.; Böhme, M.; Dapprich, S.; Gobbi, A.; Höllwarth, A.; Jonas, V.; Köhler, K. F.; Stegmann, R.; Veldkamp, A.; Frenking, G. A set of f-polarization functions for pseudo-potential basis sets of the transition metals Sc-Cu, Y-Ag and La-Au. *Chem. Phys. Lett.* **1993**, *208*, 111−114.

https://doi.org/10.1021/acscatal.3c01407
ACS Catal. 2023, 13, 9025−9032